Variability in Temperature Extremes Across the Tibetan Plateau and its Non-uniform Responses to Different ENSO Types

Zhiwei Yong
Southwest Petroleum University, school of Geoscience and Technology
Zegen Wang
Southwest Petroleum University, school of Geoscience and Technology
Junnan Xiong (neu_xjn@163.com)
School of Civil Engineering and Geomatics, Southwest Petroleum University https://orcid.org/0000-0001-6997-838X
Chongchong Ye
State Key Laboratory of Earth Surface Processes and Resource Ecology
Huaizhang Sun
Sun Yat-Sen University, school of Geography and Planning
Shaojie Wu
Institute of Aerospace Information Applications, Co,. Ltd.

Research Article

Keywords: Temperature extremes, Eastern-Pacific ENSO, Central-Pacific ENSO, Atmospheric circulation anomalies, Tibetan Plateau

Posted Date: October 20th, 2021

DOI: https://doi.org/10.21203/rs.3.rs-991974/v1

Version of Record: A version of this preprint was published at Climatic Change on June 29th, 2023. See the published version at https://doi.org/10.1007/s10584-023-03566-5.

Abstract

The variability of extreme temperatures has an important influence on the sensitive ecosystem and human activities on the Tibetan Plateau (TP). Nevertheless, the uncertainties of different El Niño-Southern Oscillation (ENSO) effects on extreme temperatures on the TP are poorly understood. Thus, this study focuses on variations in temperature extremes across the TP during 1980–2015 based on the daily maximum temperature, and minimum temperature. Then, we quantitatively examined the different effects of different ENSO types and related large-scale atmospheric circulation variables on the changes in temperature extremes. The results show that more intense and more frequent warm extremes, less intense and less frequent cold extremes were observed from 1980 to 2015. It was observed that cold extremes exhibited significant variations. In particular, the area with a significant increase in the minimum daily minimum temperature accounted for 72% of the area of the TP. Moreover, our results also suggested that there was an asymmetric relationship between temperature extremes and different ENSO types (the Eastern Pacific (EP) and Central Pacific (CP) ENSO events). especially the significant increase of cold extreme during EP El Niño episodes (slopes of frequency and intensity of cold extremes were 6.58 and -1.03). In addition, the different ENSO types had a zonal influence on temperature extreme variability on the TP through the modulation of large-scale atmospheric circulation. The changes in the intensity and frequency of the extreme warm events on the southeastern TP were distinct during the EP E1 Niño years, while the extreme warm events during the CP E1 Niño years tended to occur more frequently on the central of TP. Furthermore, the cold extremes over the western TP have experienced decreasing trends in EP La Niña years, while the frequency of warm extremes increased. The geopotential height anomaly and cyclonic circulation anomaly in the CP La Niña years enhanced cold extremes on the northeastern TP. In conclusion, within the context of the global warming, the different ENSO types are critical factor that influences temperature extremes on the TP due to these non-uniform responses of atmospheric circulation. This study provided some insight for understanding the dynamics of regional extreme temperatures in different ENSO episodes.

1. Introduction

The Paris Agreement put forward a goal that limits the increase in the global mean surface temperature to 1.5 ℃ in order to minimize the risks of extreme climate events (Hoegh-Guldberg et al., 2018). The global mean surface temperature was 0.87°C higher in 2006–2015 than in 1850–1900 (IPCC, 2013), which has already caused multiple observed changes in the climate system. Especially, the magnitude and intensity of climate extremes have increased around the world in recent decades, affecting the natural and human systems (IPCC, 2012). Therefore, the investigations about temperature extremes have received more and more attention worldwide due to their impacts (Byers et al., 2018). It has also been projected that more temperature extremes will increase mortality and morbidity in vulnerable groups (Dong et al., 2018), and will have an important influence on global agriculture (Vogel et al., 2019; Yan et al., 2021), vegetation phenology, and productivity (Crabbe et al., 2016). Hence, understanding the

variations in temperature extremes is crucial to ascertain the magnitude and pattern of the risks posed by global warming.

Generally, climate extremes are defined as the occurrence of a weather or climate variable at a value above (or below) a threshold value that is near the upper (or lower) ends of the observed values range of the variable (IPCC, 2012). During past periods, research on climate extremes has made great progress, especially the efforts of the Expert Team on Climate Change Detection and Indices (ETCCDI). They categorized climate extremes using percentiles and/or the frequency of days/nights exceeding certain thresholds, and they structured a set of climate extreme indices based on the daily maximum and minimum temperatures, and the daily precipitation (such as the hottest (coldest) day of the year and precipitation extremes) (Alexander et al., 2006; Sillmann et al., 2013). These climate extreme indices provide statistically robust insights into a region's local climatic conditions with high signal-to-noise ratio (Saleem et al., 2021; Zhou et al., 2016). Moreover, these climate extreme indices provide a comprehensive overview for temperature and precipitation extremes, and enable regional and global datasets (both station and gridded) to be developed in a comparable way. Hence, climate extreme indices have been widely applied in climate variability and trend studies (Zhang et al., 2011).

It should be noted that significant changes in extreme temperatures have been observed on global and some regional scales within different datasets (Alexander et al., 2006; Dong et al., 2018; Zhou et al., 2016). Since the beginning of the twentieth century, the widespread significant variations in temperature extremes in the global are consistent with the warming trends. These changes of the global are more pronounced for indices related to cold extremes than for indices related to warm extremes (Donat et al., 2013). At regional scales, drastic changes in the trends of warm and cold extremes have been reported across the Arabia, with an increasing number of warm days and nights, higher extreme temperature values, shorter cold spell durations and fewer cold days, and nights since the mid-1950s (Donat et al., 2014). A considerable increase in the frequency of warm nights was observed in the Indo-Pacific region during 1971–2005 (Caesar et al., 2011). For China, decreases in cold extremes and increases in warm extremes have also been found during 1961–2010 (Zhou et al., 2016). Several studies have demonstrated that the increasing trend of the minimum temperature index is greater than that of the maximum temperature index in Northeastern China and the Loess Plateau (Yan et al., 2015; Yu and Li, 2015).

It is important to understand the causes of the long-term trends in the observed temperature extremes and the possible influence of external forcing on the climate system (Dong et al., 2018). The variability of climate is believed to be related to several factors, especially the El Niño-Southern Oscillation (ENSO). The ENSO is a climate signal from the oceans and can trigger pronounced changes in climate across the world (Sun et al., 2016). The ENSO plays a robust role in the climate of East Asia, which has been mainly ascribed to the interactions between the ENSO and the East Asian summer and winter monsoons (Miao et al., 2019; Ying et al., 2015). One study investigated that the relationship between ENSO and mean temperature peaks a few months before the monsoon (del Rio et al., 2013). The above studies mainly focused on the impact of the average intensity of ENSO events, but the different types in ENSO were

poorly considered. ENSO events can be divided into two types, Eastern Pacific (EP) ENSO events and Central Pacific (CP) ENSO events, which have different influences on the atmospheric circulation in East Asia (Larkin and Harrison, 2005; Weng et al., 2009). It is noticed that CP ENSO events have been frequently observed in recent years (Wang et al., 2019), which may interfere with the robustness of climate predictions in East Asia. Thus, gaining a better understanding of the impact of different types of ENSO events on climate is necessary and would enable the identification of the key factors affecting climate extremes events. Furthermore, previous investigations have reported that large-scale changes in the wind speed and geopotential height are the likely causes of warm extremes that trigger severe heatwave conditions in the presence of a high-pressure system (Gao et al., 2018; Khan et al., 2019). Different climate variabilities will affect the distribution patterns of temperature extremes on a daily time scale. Therefore, in order to detect and attribute the influences of ENSO on observed changes of temperature extremes, the changes in large-scale modes of climate variability caused by the different ENSO types need to be considered.

Although some studies have investigated the variation of temperature extremes and its influence factors using CMIP5 models (Yin et al., 2019; You et al., 2018). little attention has been paid to the response of temperature extremes on the Tibetan Plateau (TP) to different ENSO types. As the largest and highest plateau on earth, the TP is extremely sensitive to warming compared to surrounding areas (Duan and Xiao, 2015), and an increasing number of climate extremes have occurred on the TP in recent decades, especially temperature extremes. The increased number of temperature extremes has exerted an important effect on this region, such as retreat of glaciers, terrestrial vegetation migration, wetland shrinkage, and encroachment upon farmlands (Yin et al., 2019). Therefore, it is of interest to explore the temporal and spatial patterns of temperature extremes over the TP, where temperature extremes are controlled by the rapid warming and unique large-scale atmospheric circulation around the TP. If we can gain a better understanding of the temporal and spatial variations of temperature extremes and their response characteristics to different ENSO types, then, we will be able to give an insight into the reasons behind the rapid changes in climate extremes, and to develop an essential scientific basis for future projections of climate extremes and climate change policy making.

In this study, we examined the variations in temperature extremes across the TP using the meteorological observational dataset, and extracted different ENSO types based on the national standard of China formulated. Then, we applied the composite analysis method to determine the influence of different ENSO types on the variation patterns of temperature extremes over the TP. The goals of this study were to accomplish the following: (1) analyzing temporal and spatial patterns of temperature extremes on the TP; and (2) investigating the influence mechanism of ENSO events on the patterns of temperature extremes on the TP.

2. Data Sources And Methods

2.1. Study area

The TP is located in southwestern China, starting from the Kunlun mountain range in the north, ending in the Himalayan mountain range in the southwest, and extending from the Qilian mountain range in the northeast to the Hengduan mountain range in the east (Sun et al., 2021). The TP has a total area of 2.5 million km^2, and is the most extensive elevated surface on Earth, with an average elevation of the TP is approximately 4500 m (Fig. 1) (Spicer et al., 2021). Due to the complex topography and high elevation of the TP, there is a corresponding gradient in the annual total precipitation from 16 mm in the northwest to 1764 mm in the southeast. In the coldest month, the average annual temperature is less than -5 ℃, and it is less than 10℃ in the warmest month (Chen et al., 2015; Huang et al., 2016). There are approximately 130–140 frost-free days. Overall, the plateau mountain climate of the TP is dominated by the westerly jet, the East Asian and South Asian monsoons, with the spatial pattern exhibiting horizontal band differentiation from warm-humid in the southeast to dry-cold in the northwest (Fig. S1) (Immerzeel and Bierkens, 2012).

2.2. Data sources

2.2.1. Meteorological datasets

Here, we provide a description of the meteorological observational dataset use in this study. The dataset for the meteorological stations was obtained from the China Meteorological Administration (http://data.cma.cn/), and it includes the daily maximum temperature, minimum temperature data for 1980–2015. Data quality control is essential before the analysis of climate because erroneous outliers have an effect on temperature trends (Yan et al., 2015). We used the RClimDex package (http://etccdi.pacificclimate.org/) in R software (R Core Development Team, R Foundation for Statistical Computing, Vienna, Austria) to perform data quality control, which is considered to be an effective method for data quality control (Li et al., 2012; Tong et al., 2019). First, we replaced the missing temperature data and the inaccurate temperature data (such as minimum temperatures that exceeded the maximum temperatures) with -99.9. Then, the outliers of the temperature data were checked. In this study, outliers were defined as daily values exceeding three times the standard deviation, and all the outliers were treated as not available. After quality control, 93 stations were maintained to study the variations in temperature extremes across the TP. The locations of the meteorological stations are shown in Fig. 1.

2.2.2. Sea surface temperature and Niño index data

The Extended Reconstructed Sea Surface Temperature (SST) V4 data were used in this study to estimate the monthly SST of the Pacific with a 2°×2° resolution. The data were acquired from the National Oceanic and Atmospheric Administration (NOAA) (https://psl.noaa.gov/data/gridded/) (Huang et al., 2015). In addition, the monthly Niño3 index (regional mean SST anomaly in the eastern tropical Pacific (150°W–90°W, 5°S–5°N), I_{n3}), Niño4 index (regional mean SST anomaly in the central tropical Pacific (160°E–150°W, 5°S–5°N), I_{n4}), and Niño3.4 index (regional mean SST anomaly in the east central tropical Pacific (170°W–120°W, 5°S–5°N), $I_{n3.4}$) for the period of December 1979 to January 2016 were obtained from Climate Indices: Monthly Atmospheric and Ocean Time-Series provided by the NOAA Physical Sciences Laboratory (https://psl.noaa.gov/data/climateindices/list/) (Yu et al., 2019).

2.3. Analytical methods

2.3.1. Calculation of extreme temperature indices

Four extreme temperature indices (the percentage of days when daily minimum temperature (TN) was < 10th percentile (TN10p); the percentage of days when daily maximum temperature (TX) was > 90th percentile (TX90p); the minimum value of the daily minimum temperature (TNn); and the maximum value of the daily maximum temperature (TXx)) were applied to investigate the variations of temperature extremes. These selected indices were defined by the ETCCDI for the identification of extreme temperature events, and have been adopted by several studies to explore the dynamics of extreme events (Alexander et al., 2006; IPCC, 2012). These four extreme temperature indices were calculated using RClimDex in R software with 1981–2010 as the base period. These indices were the calendar day 10th percentile centered on a 5-day window for the base period. Table S1 provides a detailed description of four extreme temperature indices.

Previous studies have found that elevation also has an important effect on the temperature distribution (Joly et al., 2018; Li et al., 2013); therefore, we utilized Anusplin 4.2 (Centre for Resource and Environmental Studies, Australian National University, Canberra), a method that takes elevation into consideration, to process the spatial interpolations of temperature at a 1 km resolution during 1980–2015 (Ye et al., 2020).

2.3.2. Identification for different ENSO types

In this study, different ENSO types (CP/EP ENSO events) were identified using the national standard of China formulated (Ren; et al., 2017; Wang et al., 2020). First, all the ENSO events during 1980–2015 period were chosen, and the ENSO events were identified when the 3-month smoothing average of the absolute value of the $I_{n3.4}$ reached and exceeded 0.5°C for at least 5 months ($I_{n3.4}$ of ≥ 0.5°C indicates an El Niño events, and a value of ≤ -0.5°C indicated an La Niña event). Then, we utilized the results to construct the EP and CP ENSO index (I_{EP} and I_{CP}) to classify all of the ENSO events, and the I_{EP} (I_{CP}) were defined based on I_{n3} and I_{n4}. The details of the calculations are described by Yu et al., 2019. If the absolute value of I_{EP} (I_{CP}) ≥ 0.5°C for at least 3 months, an event is defined as an EP (CP) ENSO event. Note that a value of I_{EP} (I_{CP}) ≥ 0.5°C for at least 3 months denotes an EP (CP) El Niño event, and a value of ≤ 0.5°C for at least 3 months denotes an EP (CP) La Niña event, respectively. Table 1 shows the identified results of the different types and intensities of ENSO events.

Table 1
Classification of ENSO events

El Niño events	Peak time	peak intensity	type	La Niña events	Peak time	peak intensity	type
1982-1983	198212	2.19℃	EP	1983-1984	198311	-1.11℃	CP
1986-1988	198708	1.55℃	EP	1984-1985	198412	-1.20℃	EP
1991-1992	199201	1.78℃	EP	1988-1989	198812	-1.96℃	CP
1994-1995	199412	1.17℃	CP	1995-1996	199512	-0.93℃	EP
1997-1998	199711	2.41℃	EP	1998-1901	200001	-1.67℃	EP
2002-2003	200211	1.41℃	EP	2007-2008	200801	-1.63℃	EP
2004-2005	200409	0.78℃	CP	2008-2009	200901	-0.83℃	CP
2006-2007	200611	0.99℃	EP	2010-2011	201010	-1.61℃	CP
2009-2010	200912	1.61℃	EP	2011-2012	201111	-1.05℃	EP
2015	201512	2.69℃	EP				

2.3.3. Trend analysis

We used the nonparametric Mann–Kendall statistical test to determine understand the statistical significance of the trends in extreme temperature indices in each grid, and the magnitudes of the trends were estimated using Sen's slope estimator method (Mann, 1945; Sen, 1968). The results of the nonparametric Mann–Kendall statistical test are not disturbed by outliers in the time series and are not affected by the distribution of the data. A positive slope indicates an upward trend; otherwise, the trend of the index is downward. The 5% significance level was used in all of the significance tests (Miao et al., 2019; Poudel et al., 2020). It was calculated as follows.

We applied the Mann–Kendall statistical test to a times series $X = (x_1, x_2, \ldots, x_n)$, where n is the length of the time series, The statistical test S as following Equation (1):

$$S = \sum_{i}^{n-1} \sum_{j=i+1}^{n} \operatorname{sgn}\left(X_j - X_i\right) \tag{1}$$

where X_i and X_j are the i and j values in the time series, respectively. Simultaneously, sgn is defined as Equation (2):

$$\operatorname{sgn}\left(X_i - X_j\right) = \begin{cases} 1, X_i - X_j > 0 \\ 0, X_i - X_j = 0 \\ -1, X_i - X_j < 0 \end{cases} \quad (2)$$

Then, the statistic test S is asymptotically normal, and its variance computed by Equation (3).

$$Var\,(S) = \frac{n(n-1)(2n+5) - \sum_{k=1}^{m} t_k(t_k-1)(2t_k+5)}{18} \quad (3)$$

In Equation (3), m is the number of tied groups, and t_k is the number of observations in the *k*th tied group. When the sample size is n > 10, the standard normal variable Z calculated using Equation (4):

$$Z = \begin{cases} \dfrac{S-1}{\sqrt{Var\,(S)}}, S > 0 \\ 0, \quad S = 0 \\ \dfrac{S+1}{\sqrt{Var\,(S)}}, S < 0 \end{cases} \quad (4)$$

A positive *Z* value indicates an increasing trend; while a negative *Z* value indicates a decreasing trend. In this study, the significance level was set at α = 0.05. When $|Z| \geq Z_{1-\alpha/2}$, the trend of the time series is statistically significant.

The Mann–Kendall statistical test can analyze the trend and significance of time series, but it cannot provide the magnitude of the trend. Therefore, we used Sen's slope to estimate the magnitude of the time series trend. The magnitude of the slope β was calculated from the non-parametric estimator of Sen's slope (Sen, 1968), as shown following Equation (5).

$$\beta = median\left[\frac{X_j - X_i}{j - i}, \forall i cript > \right] \quad (5)$$

The Mann–Kendall statistical test and Sen's slope were applied to extreme temperature indices described above to obtain the trends and their significances during 1980–2015.

2.3.4. Composite analysis

To assess the role of climate variability (such as the ENSO), we used a composite analysis method to provide a direct representation of the possible influences of the different ENSO types on the spatial and temporal variations in temperature extremes. The method is similar to that used in previous studies (Miao et al., 2019; Zhang et al., 2010). In the study, we selected the years with the five highest and five lowest I_{EP} and I_{CP} values. We computed the means of the extreme temperature indices (T_{high} and T_{low}) for the high- and low-EP/CP ENSO index years from 1980 to 2015, and the 30-year means of extreme temperature indices (T_{mean}) during the base period (1980-2010). Then, we calculated the difference in these averages (T_{high} - T_{mean} or T_{low} - T_{mean}) to determine the influences of the different ENSO events types. Moreover, we used the two-sided Student's t test to determine the statistical significance of the composite differences.

3. Results

3.1. Temporal and spatial patterns of the temperature extremes

Figure 2 shows the mean annual changes in the four extreme temperature indices (TN10p, TX90p, TNn, TXx) across the TP. Inspecting Fig. 2a, the mean annual TN10p significantly decreased ($p < 0.001$) at a rate of -0.38 day/year. However, the mean annual TX90p, TNn, and TXx display significantly increasing trends across the TP during the period of 1980-2015, with slopes of 0.32 day/year, 0.05 ℃/year, and 0.04 ℃/year, respectively (Figs. 2b, 2c and 2d). Overall, the frequency of the extreme events related to low temperatures significantly decreased on the TP, while frequency of the extreme events associated with high temperatures significantly increased.

Figure 3 illustrates that the spatial patterns of TN10p, TX90p, TNn, TXx trends on the TP during 1980–2015. The TN10p trend is spatially consistent across the TP, with significant decreasing trends over the most of the TP (Fig. S2a). The annual changes ranged from -0.77 to -0.07 day/year, with the strongest decreases occurring on the western TP (Fig. 3a). In addition, TNn increased on the most regions of TP (Fig. 3b). The TNn significantly increased over the central and eastern TP, accounting for 72% of the total area of the TP (Fig. S2b). Figs. 3c and Fig. S2c show that the TX90p statistically significantly increased over the entire TP. The TXx varied from approximately-0.13 to 0.15 day/year (Fig. 3d), with a significant increase over 29% of the area. The western and eastern parts of the TP had the highest rate of increase, and a significant decrease trend occurred in a small part of the southern TP (Fig. S2d).

3.2. Response of temperature extremes to different ENSO types.

Figure S3 shows the time series of the monthly $I_{n3.4}$, I_{EP}, and I_{CP} from 1980 to 2015. The time series indicate that the SST anomalies caused by the CP ENSO events were weaker than those caused by the EP ENSO events. Based on the time series data for the I_{EP}, and $I_{CP,}$ we used the national standard of China formulated to identify the different ENSO types during the period of 1980-2015. The detailed results are

presented in Table 1. With regard to the frequency of ENSO events, the frequency of EP El Niño events (eight events) was greater than that of CP El Niño events (two events) in 36-year study period. However, the frequency of EP La Niña events (five events) was similar to that of CP La Niña events (four events). Furthermore, these events also reflect distinct seasonal characteristics, and the ENSO events tended to mature in winter and gradually decline in the following year.

Next, we further explored the response characteristics of temperature extremes to the different ENSO types. Fig. 4 shows the detailed relationships between extreme temperature indices and I_{EP} (I_{CP}). The magnitude of EP El Niño episodes was observed to strongly influence the frequency and intensity of cold extremes on the TP, with the slope of TN10p being 6.58 and that of TNn being -1.03 (Figs. 4a and 4e). In addition, the slopes of I_{EP} and TX90p (TXx) were -7.27 and -0.76 during the cold phases of the ENSO, respectively (Figs. 4c and 4g). This implies that the EP El Niño episodes resulted in more cold extremes, but fewer warm extremes occurred during the EP La Niña episodes. In contrast, the correlations with the CP ENSO episodes were smaller and relatively insignificant. For the CP La Niña events, these positive slopes and correlation coefficients are dominated by the TNn (TXx) and I_{CP}, but the positive relationships are not both robust for the years with $I_{CP} < 0$ and $I_{CP} > 0$ (Figs. 4f and 4h). Moreover, the correlations between the CP El Niño episodes and temperature extremes were smaller and relatively insignificant on the TP (Figs. 4d, 4f and 4h). These results are suggestive of an asymmetric response characteristic of temperature extremes over the TP to the different ENSO types.

3.3. Non-uniform influence of the different ENSO types.

We applied a composite analysis method to assess the spatial response characteristics of temperature extremes to the different ENSO types. Fig. 5 shows the composite differences between the average of the E1 Niño years and the base period, based on I_{EP}, and I_{CP}. Compared with the base period, the TN10p in the EP E1 Niño years tended to be greater over large areas of the southern TP (Fig. 5a), and significant decreasing trends occurred over the northern part of the TP, especially in the Qaidam Basin (Fig. S5a). However, the TX90p in the EP E1 Niño years exhibited the opposite trend in similar regions (Fig. 5c). In terms of the intensity of temperature extremes on the TP, the TNn was greater in the EP E1 Niño years than during the based period over the northern TP (Fig. 5b), with the difference values ($T_{high} - T_{mean}$) being statistically significant at the 95% confidence level (Fig. S5c). The significant increasing trends were scatted in some of the grids in the southeastern region of the TP (Fig. S5d), but the variation in the magnitude of the TXx (-1.88 to 1.81 ℃) was less than the TNn (-2.45 to 2.01 ℃) for the entire TP (Fig. 5d).

However, the differences in the magnitude of the change in temperature extremes in some areas were quite large for both types of events. The TN10p during the CP E1 Niño years tended to decrease over large parts of the TP, with the lowest value being -5.92 days (Fig. 6a). The significant decrease occurred in the western TP, and in some grids in the northeastern and southeastern TP (Fig. S6a). Compared with the TN10p, the TX90p exhibited the opposite patterns on the TP (Fig. 6c), and the TX90p in the CP E1 Niño years tended to be greater over the central region of the TP (Fig. S6c). In addition, the CP events caused a

large increase in the TNn over the majority of the TP, with the maximum change of > 3℃ (Fig. 6b). For most of the grids in the northern and central TP, the TXx values tended to be greater during the CP E1 Niño years than during the based period, and the decreasing grids were scattered in the southwest and southeastern TP (Fig. 6d).

With regard to the response of temperature extremes to the different La Niña types, it was observed that the TN10p in the EP La Niña years tended to be lower over large areas of the TP, with the regional mean value of -1.58 day (Fig. 7a). In stark contrast, the TX90p in the EP La Niña years was significantly greater than that during the base period, ranging from -0.44 to 8.58 days (Fig. 7c). The regions with significant increases were located in the western, central, and southeastern TP (Fig. S7c). It was obvious that the variation in the TNn displayed spatial heterogeneity, the increasing grids were distributed in the western TP (the maximum values of > 1.5 ℃), and the decreasing area is found in northern TP (the minimum of < -1.0 ℃) (Fig. 7b). Fig. 7d shows that the TXx in the EP La Niña years was greater than during the base period in some scattered regions of the northwestern, southern, and eastern TP, with a maximum of 2.08 ℃.

In addition, a clear variation is apparent in temperature extremes on the TP in the CP La Niña years. Fig. 8a demonstrates that the TN10p was larger during the CP La Niña years than the base period on the northern TP, and the areas with lower values were observed on the northwestern and southern edge of the TP. The variation in the TN10p ranged from -4.44 to 3.04 days. The TX90p in the CP La Niña years increased in large parts of the eastern TP, some grids in the southwestern, and northern TP (Fig. 8c), but most of these changes were not statistically significant (Fig. S8c). The regional mean of the TNn on the TP was > -0.51℃ during the CP La Niña years, and the decreasing trends were located in the northeastern and western TP (Fig. 8b). The minimum TXx during the CP La Niña years is distributed in the southwestern TP, and the high value regions were observed in the western edge and the northwestern, and northeastern parts of the TP (Fig. 8d).

3.4. Effects of large-scale atmospheric circulation

Figure 9 depicts the anomalies in the geopotential height and wind at 500 hPa caused by the different ENSO events. The EP El Niño events resulted in positive geopotential height anomalies at 500 hPa over Lake Baikal and northern China, and negative geopotential height anomalies over the southern China and the western TP (Fig. 9a). However, there were differences in the intensities and locations of the geopotential height anomalies formed in response to the CP El Niño events. Positive geopotential height anomalies centered on Japan, and northeastern, and western China. The negative geopotential height anomalies centered to the western Pacific and Bangladesh can be detected. These geopotential height anomalies favored the prevalence of easterly winds over the TP (Fig. 9b). The negative geopotential height over northern India and the easterly winds induced warm humid flows that benefited the existence of snow cover over the TP, which offset the cold conditions across the majority of the TP. Next, we discuss the distinctive impacts of the two types of La Niña events. Fig. 9c indicated significantly opposite geopotential height patterns between EP El Niño events and EP La Niña events, and that the TP was dominated by northwesterly winds. A positive geopotential height anomaly and a cyclonic circulation

anomaly were observed around the western TP. Furthermore, the geopotential height anomalies during the CP La Niña events were opposite to those during the El Niño events, except for the positive height anomalies over the western TP (Fig. 9d). A negative geopotential height anomaly and a cyclonic circulation anomaly occurred on the northeastern TP during the CP La Niña events, leading one to expect a decrease in temperature on the northeastern TP.

4. Discussion

4.1. Variability of extreme temperatures on the TP

This paper presents an analysis of the spatial and temporal variabilities in temperature extremes across the TP during 1980–2015. The response characteristics of temperature extremes to different ENSO types, and the related atmospheric circulation variations during years with different ENSO types were examined to explore the underlying mechanisms driving these changes.

The mean value of the significant trends was -0.38 day/year for the TN10p. However, the opposite trends were observed for the TX90p, TNn, and TXx from 1980 to 2015 (Fig. 2). These results indicate that the frequency and intensity of the warm extremes on the TP increased during the 36-year study period, while the intensity and frequency of the cold extremes decreased. Previous studies have reported similar variations in the temperature extremes in China, Asia and the global (Alexander et al., 2006; Dong et al., 2018; Zhou et al., 2016), and all of the variations in temperature extremes on the TP are larger than those in the other regions of China (Yin et al., 2019). The main reason for this difference is that due to the surface albedo reduction caused by the reduced snow cover under global warming, the surface albedo feedback can warm the surface air by absorbing more solar radiation and then emitting more longwave radiation upward (Ding et al., 2018; Kang et al., 2010). Moreover, the radiative forcing effect of greenhouse gases can also cause significant air warming (Aguilar et al., 2009).

Our results indicate that the variations in the four extreme temperature indices were not spatially uniform on the TP. The TN10p shows significant decreasing trends over most of the TP, while the TX90p displays statistically significant increasing trends (Fig. S2). These results reflect the decreasing frequency of the extreme cold events and the increasing frequency of the extreme warm events over the entire TP, which is consistent with the mean values of the significant changes in the TN10p (TX90p) on the TP (Fig. 2). Furthermore, the intensity of temperature extremes shows significant regional variations, and the areas in which the TNn significantly increased were in the central and eastern TP (Fig. S2). The possible reasons for this are related to the pattern of the amounts of clouds above the TP. The variations in the cloud amount play an essential role in the energy balance and thus the temperature distribution (Ding et al., 2018). During 1961-2003, the amount of low-level clouds demonstrated a significant increasing trend over the central and eastern TP in the nighttime, which led to enhanced atmospheric counter radiation and weakened the effective terrestrial radiation, further warming the surface air on winter nights (Duan and Wu, 2006). These results suggest that temperature extremes have become more homogenous and widespread across the TP.

4.2. Non-uniform response of extreme temperature to different ENSO types

Both tropical and mid-latitude ocean signals can affect the thermal conditions on the TP (Liu et al., 2020). In particular, ENSO events are a major factor controlling the variability of climate at a global scale because they modulate the variability in global atmospheric circulation (Miao et al., 2019). Our results demonstrate that there is an asymmetric relationship between temperature extremes over the TP and the different ENSO types. For r the EP ENSO events, the EP El Niño episodes result in more extreme cold events, while EP La Niña episodes result in fewer extreme warm events. However, the correlations between the CP ENSO episodes and temperature extremes are smaller and relatively insignificant on the TP (Fig. 4). This asymmetric response characteristics are owing to the nonlinear effects of the ENSO events (Li et al., 2021).

Notably, the different types of ENSO events have non-uniform influences on the changes in both the intensity and frequency of in temperature extremes. The changes in the intensity and frequency of the extreme warm events on the southeastern TP were distinct during the EP E1 Niño years, which may be attributed to the circulation anomalies in southwestern China, which induce southeasterlies over the southeastern TP to offset the local extreme cold events (Fig. 9a). Moreover, the concurrence of a higher water-vapor flux and changes of the subtropical high during E1 Niño years could enhance the differences in air temperature variability on the southeastern and other regions of the TP. Although the extreme warm events during the CP E1 Niño years tended to occur more frequently on the central of TP, but there were some extreme cold events on the eastern and southeastern TP (Fig. 5). The large-scale atmospheric circulation revealed that the CP El Niño events resulted a positive geopotential height anomaly centered to Japan and northeastern China, and negative geopotential height anomalies centered over the western Pacific and Bangladesh. These geopotential height anomalies favored the prevalence of the easterly winds over the TP (Fig. 9b). The negative geopotential height over northern India and the easterly winds can induce warm humid flows, which offset the cold conditions across the majority of the TP (Liu et al., 2020; Wang et al., 2020). As a result, anomalously warm and humid conditions can be experienced around the TP.

Furthermore, our results indicate that the frequency and intensity of cold extremes over the western TP has experienced decreasing trends in EP La Niña years, while the frequency of warm extremes increased (Fig. 7). Based on the large-scale atmospheric circulation in the EP La Niña years, we observed that the anomalous southerly winds near the western TP weakened the northwesterly, and the weak northwesterly corresponded to fewer extreme cold events over the western TP (Fig. 9c). The weakened wind in conjunction with the strengthened geopotential height, was largely responsible for the above atmospheric anomalies tied to the increased warm extremes in the EP La Niña years. Moreover, we also found that the changes in the temperature extremes were stronger during the EP La Niña years than during the EP E1 Niño years, which is consistent with the results of Saleem et al., (2021). Nevertheless, the geopotential height anomaly and cyclonic circulation anomaly in the CP La Niña years did not resemble those in the

EP La Niña years, which led to differences in the variability of the temperature extremes. Especially, the enhanced cold extremes were observed on the northeastern TP (Fig. 8). The resulting large-scale atmospheric circulation in the CP La Niña years demonstrates that a negative geopotential height anomaly and a cyclonic circulation anomaly occurred over the northeastern TP, triggering weakened easterly winds and significant westerlies (Fig. 9d, Fig. S9d). This result suggests the existence stronger of mid-tropospheric cold air activities over these areas (Wang et al., 2020).

4.3. Importance and uncertainties

In summary, the different types of ENSO events and the large-scale atmospheric circulations they cause likely play an important role in the variability of temperature extremes on the TP on both spatial and temporal scales. In this study, we divided the ENSO types based on the values of the EP (CP) ENSO indices. The different ENSO types may result in the observed asymmetries, and the ENSO events influence on the non-uniform spatial patterns of temperature extremes across the TP. Non-uniform changes in the precipitation intensity have also been observed (Karori et al., 2013; Miao et al., 2019). In addition, in this study, how ENSO events modulate the variability of the temperature extremes on the TP through large-scale atmospheric circulation was explored. The observed spatial heterogeneity in temperature extremes during the different types of ENSO events indicates that there is a high risk of drought and other natural hazards occurring in different regions during the years with different ENSO types. However, it should be noted that uncertainties may occur if only the different ENSO events are used to conduct climate change forecasts. Previous investigations have reported that other factors can affect local microclimates and the changes of temperature extremes, for example, precipitation (Bao et al., 2017; Yong et al., 2021), elevation (Liu et al., 2009), topographic heterogeneity (Sun and Zhang, 2016), and anthropogenic aerosols (Seong et al., 2021). However, the underlying mechanisms controlling the variations in the temperature extremes caused by complex factors are still ambiguous, future researches are required to analyze the interactions between the different influence factors. As more frequent ENSO events are predicted to occur in the future (Wang et al., 2019), it may be possible to obtain more robust prediction results based on the interactions between ENSO events and other influencing factors in the future.

5. Conclusions

This study focused on the variability of temperature extremes across the TP and its response to different ENSO types. Specifically, the results of this study indicate that all the extreme indices show distinct warming trends. More intense and more frequent warm extremes, less intense and less frequent cold extremes have occurred on the TP since the 1980s. Therein, the intensity of cold extremes also exhibited significant regional variation, and the areas with significantly increased TNn values were distributed on the central and eastern TP, the possible reason for the result is related to the patterns in amounts of clouds. Next, the different response characteristics of temperature extremes to different ENSO events, and their related large-scale atmospheric circulation anomalies were analyzed. Our results also suggest that there is an asymmetric relationship between temperature extremes over the TP and the different ENSO

types. Specially, the significant increasing of cold extreme during EP El Niño episodes, with the slopes of frequency and intensity of cold extremes are 6.58 and -1.03, respectively. Nevertheless, the slopes of other ENSO types with temperature extremes are smaller and relatively insignificant on the TP. Different ENSO types may result in different regional atmospheric circulation anomalies, and thus, they have a non-uniform influence on temperature extremes across the TP. The variations of the extreme warm events on the southeastern TP were distinct during the EP E1 Niño years, while the extreme warm events during the CP E1 Niño years showed significantly increasing trend on the central of the TP. Furthermore, the cold extremes over the western TP have tended to decreasing in EP La Niña years, while the frequency of warm extremes increased. The geopotential height anomaly and cyclonic circulation anomaly in the CP La Niña years enhanced cold extremes on the northeastern TP. This study highlights the non-uniform variations of temperature extremes over the TP during years with different ENSO types. The changed in temperature extremes due to the different ENSO episodes are vitally important for regional climate predictions. The benefits of improved regional climate prediction are enormous for the sensitive ecosystems and agriculture on the TP. In the future, incorporating the differences in the SST anomaly patterns and other influence factors will be helpful for producing robust temperature extreme predictions for the TP.

References

1. Aguilar E, Aziz Barry A, Brunet M, Ekang L, Fernandes A, Massoukina M et al. Changes in temperature and precipitation extremes in western central Africa, Guinea Conakry, and Zimbabwe, 1955–2006. Journal of Geophysical Research: Atmospheres 2009; 114. https://doi.org/10.1029/2008JD011010
2. Alexander LV, Zhang X, Peterson TC, Caesar J, Gleason B, Klein Tank AMG et al. Global observed changes in daily climate extremes of temperature and precipitation. J Geophys Res 2006; 111. https://doi.org/10.1029/2005JD006290
3. Bao J, Sherwood SC, Alexander LV, Evans JP (2017) Future increases in extreme precipitation exceed observed scaling rates. Nat Clim Chang 7:128–132. https://doi.org/10.1038/nclimate3201
4. Byers E, Gidden M, Leclère D, Balkovic J, Burek P, Ebi K et al. Global exposure and vulnerability to multi-sector development and climate change hotspots. Environ Res Lett. 2018; 13: 055012. https://doi.org/ 10.1088/1748-9326/aabf45
5. Caesar J, Alexander L, Trewin B, Tse-Ring K, Sorany L, Vuniyayawa V et al (2011) Changes in temperature and precipitation extremes over the Indo-Pacific region from 1971 to 2005. Int J Climatol 31:791–801. https://doi.org/10.1002/joc.2118
6. Chen X, An S, Inouye DW, Schwartz MD (2015) Temperature and snowfall trigger alpine vegetation green-up on the world's roof. Glob Change Biol 21:3635–3646. https://doi.org/10.1111/gcb.12954
7. Crabbe RA, Dash J, Rodriguez-Galiano VF, Janous D, Pavelka M, Marek MV (2016) Extreme warm temperatures alter forest phenology and productivity in Europe. Sci Total Environ 563:486–495. https://doi.org/10.1016/j.scitotenv.2016.04.124

8. del Rio S, Anjum Iqbal M, Cano-Ortiz A, Herrero L, Hassan A, Penas A (2013) Recent mean temperature trends in Pakistan and links with teleconnection patterns. Int J Climatol 33:277–290. https://doi.org/10.1002/joc.3423
9. Ding J, Cuo L, Zhang Y, Zhu F (2018) Monthly and annual temperature extremes and their changes on the Tibetan Plateau and its surroundings during 1963–2015. Sci Rep 8:1–23. https://doi.org/10.1038/s41598-018-30320-0
10. Donat M, Alexander L, Yang H, Durre I, Vose R, Dunn R et al (2013) Updated analyses of temperature and precipitation extreme indices since the beginning of the twentieth century: The HadEX2 dataset. Journal of Geophysical Research: Atmospheres 118:2098–2118. https://doi.org/10.1002/jgrd.50150
11. Donat M, Peterson T, Brunet M, King A, Almazroui M, Kolli R et al (2014) Changes in extreme temperature and precipitation in the Arab region: long-term trends and variability related to ENSO and NAO. Int J Climatol 34:581–592. https://doi.org/10.1002/joc.3707
12. Dong S, Sun Y, Aguilar E, Zhang X, Peterson TC, Song L et al (2018) Observed changes in temperature extremes over Asia and their attribution. Clim Dyn 51:339–353. https://doi.org/10.1007/s00382-017-3927-z
13. Duan A, Wu G. Change of cloud amount and the climate warming on the Tibetan Plateau. Geophys Res Lett. 2006; 33. https://doi.org/10.1029/2006GL027946
14. Duan A, Xiao Z (2015) Does the climate warming hiatus exist over the Tibetan Plateau? Sci. Rep 5:1–9. https://doi.org/10.1038/srep13711
15. Gao M, Wang B, Yang J, Dong W (2018) Are peak summer sultry heat wave days over the Yangtze–Huaihe River basin predictable? J Clim 31:2185–2196. https://doi.org/10.1175/JCLI-D-17-0342.1
16. Hoegh-Guldberg O, Jacob D, Bindi M, Brown S, Camilloni I, Diedhiou A et al. Impacts of 1.5 C global warming on natural and human systems. Global warming of 1.5 C. An IPCC Special Report 2018
17. Huang B, Banzon VF, Freeman E, Lawrimore J, Liu W, Peterson TC et al (2015) Extended Reconstructed Sea Surface Temperature Version 4 (ERSST.v4). Part I: Upgrades and Intercomparisons. J Clim 28:911–930. https://doi.org/10.1175/JCLI-D-14-00006.1
18. Huang K, Zhang Y, Zhu J, Liu Y, Zu J, Zhang J (2016) The influences of climate change and human activities on vegetation dynamics in the Qinghai-Tibet Plateau. Remote Sens 8:876. https://doi.org/10.3390/rs8100876
19. Immerzeel WW, Bierkens MFP (2010) Asian Water Towers: More on Monsoons—Response. Science 330(6004):585. https://doi.org/10.1126/science.330.6004.585-a
20. IPCC (2012) Managing the Risks of Extreme Events and Disasters to Advance Climate Change Adaptation. A Special Report of Working Groups I and II of the Intergovernmental Panel on Climate Change. Cambridge, pp. 582
21. IPCC (2013) Climate Change 2013: The Physical Science Basis: Working Group I Contribution to the Fifth Assessment Report of the Intergovernmental Panel on Climate Change, Cambridge, pp. 159-254
22. Joly D, Castel T, Pohl B, Richard Y (2018) Influence of spatial information resolution on the relation between elevation and temperature. Int J Climatol 38:5677–5688. https://doi.org/10.1002/joc.5771

23. Kang S, Xu Y, You Q, Flügel W-A, Pepin N, Yao T (2010) Review of climate and cryospheric change in the Tibetan Plateau. Environ Res Lett 5:015101. https://doi.org/10.1088/1748-9326/5/1/015101
24. Karori MA, Li J, Jin F-F (2013) The asymmetric influence of the two types of El Niño and La Niña on summer rainfall over southeast China. J Clim 26:4567–4582. https://doi.org/10.1175/JCLI-D-12-00324.1
25. Khan N, Shahid S, Juneng L, Ahmed K, Ismail T, Nawaz N (2019) Prediction of heat waves in Pakistan using quantile regression forests. Atmos Res 221:1–11. https://doi.org/10.1016/j.atmosres.2019.01.024
26. Larkin NK, Harrison D. On the definition of El Niño and associated seasonal average US weather anomalies. Geophys Res Lett 2005; 32. https://doi.org/10.1029/2005GL022738
27. Li G, Gao C, Lu B, Chen H (2021) Inter-annual variability of spring precipitation over the Indo-China Peninsula and its asymmetric relationship with El Niño-Southern Oscillation. Clim Dyn 56:2651–2665. https://doi.org/10.1007/s00382-020-05609-4
28. Li X, Wang L, Chen D, Yang K, Xue B, Sun L (2013) Near-surface air temperature lapse rates in the mainland China during 1962–2011. Journal of Geophysical Research: Atmospheres 118:7505–7515. https://doi.org/10.1002/jgrd.50553
29. Li Z, He Y, Wang P, Theakstone WH, An W, Wang X et al (2012) Changes of daily climate extremes in southwestern China during 1961–2008. Glob Planet Change 80:255–272. https://doi.org/10.1016/j.gloplacha.2011.06.008
30. Liu X, Cheng Z, Yan L, Yin Z-Y (2009) Elevation dependency of recent and future minimum surface air temperature trends in the Tibetan Plateau and its surroundings. Glob Planet Change 68:164. https://doi.org/10.1016/j.gloplacha.2009.03.017
31. Liu Y, Lu M, Yang H, Duan A, He B, Yang S et al (2020) Land–atmosphere–ocean coupling associated with the Tibetan Plateau and its climate impacts. Natl Sci Rev 7:534–552. https://doi.org/10.1093/nsr/nwaa011
32. Mann H (1945) Nonparametric Tests Against Trend. Econometrica 13(3):245–259. https://doi.org/10.2307/1907187
33. Miao C, Duan Q, Sun Q, Lei X, Li H (2019) Non-uniform changes in different categories of precipitation intensity across China and the associated large-scale circulations. Environ Res Lett 14:025004. https://doi.org/10.1088/1748-9326/aaf306
34. Poudel A, Cuo L, Ding J, Gyawali AR (2020) Spatio-temporal variability of the annual and monthly extreme temperature indices in Nepal. Int J Climatol 40:4956–4977. https://doi.org/10.1002/joc.6499
35. Ren H, Sun; c, Ren; F, Yuan; Y, Lu; B, Tian; B, et al. Identification method for El Niño/La Niña events. Standards Press of China, Beijing, 2017, pp. 1–6
36. Saleem F, Zeng X, Hina S, Omer A (2021) Regional changes in extreme temperature records over Pakistan and their relation to Pacific variability. Atmos Res 250:105407. https://doi.org/10.1016/j.atmosres.2020.105407

37. Sen PK (1968) Estimates of the regression coefficient based on Kendall's tau. Journal of the American statistical association 63:1379–1389. https://doi.org/10.1080/01621459.1968.10480934
38. Seong M-G, Min S-K, Kim Y-H, Zhang X, Sun Y (2021) Anthropogenic Greenhouse Gas and Aerosol Contributions to Extreme Temperature Changes during 1951–2015. J Clim 34:857–870. https://doi.org/10.1175/JCLI-D-19-1023.1
39. Sillmann J, Kharin V, Zhang X, Zwiers F, Bronaugh D (2013) Climate extremes indices in the CMIP5 multimodel ensemble: Part 1. Model evaluation in the present climate. Journal of Geophysical Research: Atmospheres 118:1716–1733. https://doi.org/10.1002/jgrd.50203
40. Spicer RA, Su T, Valdes PJ, Farnsworth A, Wu F-X, Shi G et al (2021) Why 'the uplift of the Tibetan Plateau'is a myth. Natl Sci Rev 8:nwaa091. https://doi.org/10.1093/nsr/nwaa091
41. Sun J, Zhan T, Liu M, Zhang Z, Wang Y, Liu S et al (2021) Verification of the biomass transfer hypothesis under moderate grazing across the Tibetan plateau: a meta-analysis. Plant Soill 458:139–150. https://doi.org/10.1007/s11104-019-04380-8
42. Sun Q, Miao C, AghaKouchak A, Duan Q (2016) Century-scale causal relationships between global dry/wet conditions and the state of the Pacific and Atlantic Oceans. Geophys Res Lett 43:6528–6537. https://doi.org/10.1002/2016GL069628
43. Sun R, Zhang B (2016) Topographic effects on spatial pattern of surface air temperature in complex mountain environment. Environ Earth Sci 75:621. https://doi.org/10.1007/s12665-016-5448-1
44. Tong S, Li X, Zhang J, Bao Y, Bao Y, Na L et al (2019) Spatial and temporal variability in extreme temperature and precipitation events in Inner Mongolia (China) during 1960–2017. Sci Total Environ 649:75–89. https://doi.org/10.1016/j.scitotenv.2018.08.262
45. Vogel E, Donat MG, Alexander LV, Meinshausen M, Ray DK, Karoly D et al (2019) The effects of climate extremes on global agricultural yields. Environ Res Lett 14:054010. https://doi.org/10.1088/1748-9326/ab154b
46. Wang B, Luo X, Yang Y-M, Sun W, Cane MA, Cai W et al. Historical change of El Niño properties sheds light on future changes of extreme El Niño. Proc. Natl. Acad. Sci. U. S. A. 2019; 116: 22512-22517. https://doi.org/10.1073/pnas.1911130116
47. Wang J, Liu Y, Ding Y (2020) On the connection between interannual variations of winter haze frequency over Beijing and different ENSO flavors. Sci Total Environ 740:140109. https://doi.org/10.1016/j.scitotenv.2020.140109
48. Weng H, Behera SK, Yamagata T (2009) Anomalous winter climate conditions in the Pacific rim during recent El Niño Modoki and El Niño events. Clim Dyn 32:663–674. https://doi.org/10.1007/s00382-008-0394-6
49. Yan G, Qi F, Wei L, Aigang L, Yu W, Jing Y et al (2015) Changes of daily climate extremes in Loess Plateau during 1960–2013. Quat Int 371:5–21. https://doi.org/10.1016/j.quaint.2014.08.052
50. Yan Y, Jeong S, Park C-E, Mueller ND, Piao S, Park H et al (2021) Effects of extreme temperature on China's tea production. Environ Res Lett 16:044040. https://doi.org/10.1088/1748-9326/abede6

51. Ye C, Sun J, Liu M, Xiong J, Zong N, Hu J et al (2020) Concurrent and Lagged Effects of Extreme Drought Induce Net Reduction in Vegetation Carbon Uptake on Tibetan Plateau. Remote Sens 12:2347. https://doi.org/10.3390/rs12152347
52. Yin H, Sun Y, Donat MG (2019) Changes in temperature extremes on the Tibetan Plateau and their attribution. Environ Res Lett 14:124015. https://doi.org/10.1088/1748-9326/ab503c
53. Ying K, Zhao T, Quan X-W, Zheng X, Frederiksen CS (2015) Interannual variability of autumn to spring seasonal precipitation in eastern China. Clim Dyn 45:253–271. https://doi.org/10.1007/s00382-014-2411-2
54. Yong Z, Xiong J, Wang Z, Cheng W, Yang J, Pang Q (2021) Relationship of extreme precipitation, surface air temperature, and dew point temperature across the Tibetan Plateau. Clim Change 165:1–22. https://doi.org/10.1007/s10584-021-03076-2
55. You Q, Jiang Z, Wang D, Pepin N, Kang S (2018) Simulation of temperature extremes in the Tibetan Plateau from CMIP5 models and comparison with gridded observations. Clim Dyn 51:355–369. https://doi.org/10.1007/s00382-017-3928-y
56. Yu X, Wang Z, Zhang H, Zhao S (2019) Impacts of different types and intensities of El Niño events on winter aerosols over China. Sci Total Environ 655:766–780. https://doi.org/10.1016/j.scitotenv.2018.11.090
57. Yu Z, Li X (2015) Recent trends in daily temperature extremes over northeastern China (1960–2011). Quat. Int 380:35–48. https://doi.org/10.1016/j.quaint.2014.09.010
58. Zhang X, Alexander L, Hegerl GC, Jones P, Tank AK, Peterson TC et al (2011) Indices for monitoring changes in extremes based on daily temperature and precipitation data. WIREs Clim Change 2:851–870. https://doi.org/10.1002/wcc.147
59. Zhang X, Wang J, Zwiers FW, Groisman PY (2010) The influence of large-scale climate variability on winter maximum daily precipitation over North America. J Clim 23:2902–2915. https://doi.org/10.1175/2010JCLI3249.1
60. Zhou B, Xu Y, Wu J, Dong S, Shi Y (2016) Changes in temperature and precipitation extreme indices over China: Analysis of a high-resolution grid dataset. Int J Climatol 36:1051–1066. https://doi.org/10.1002/joc.4400

Figures

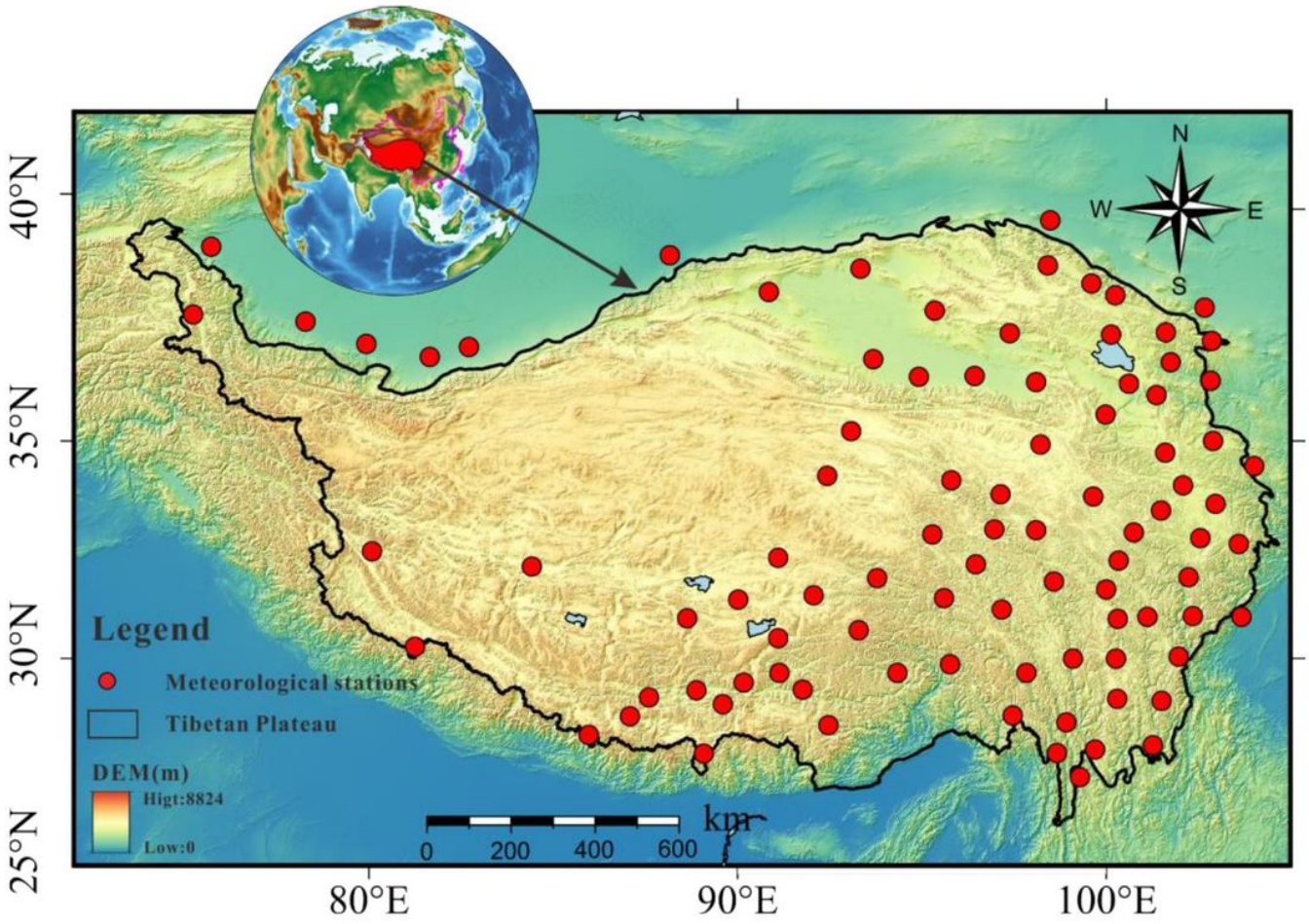

Figure 1

The study area, and the locations of meteorological stations, and the geographical position of the Tibetan Plateau in China.

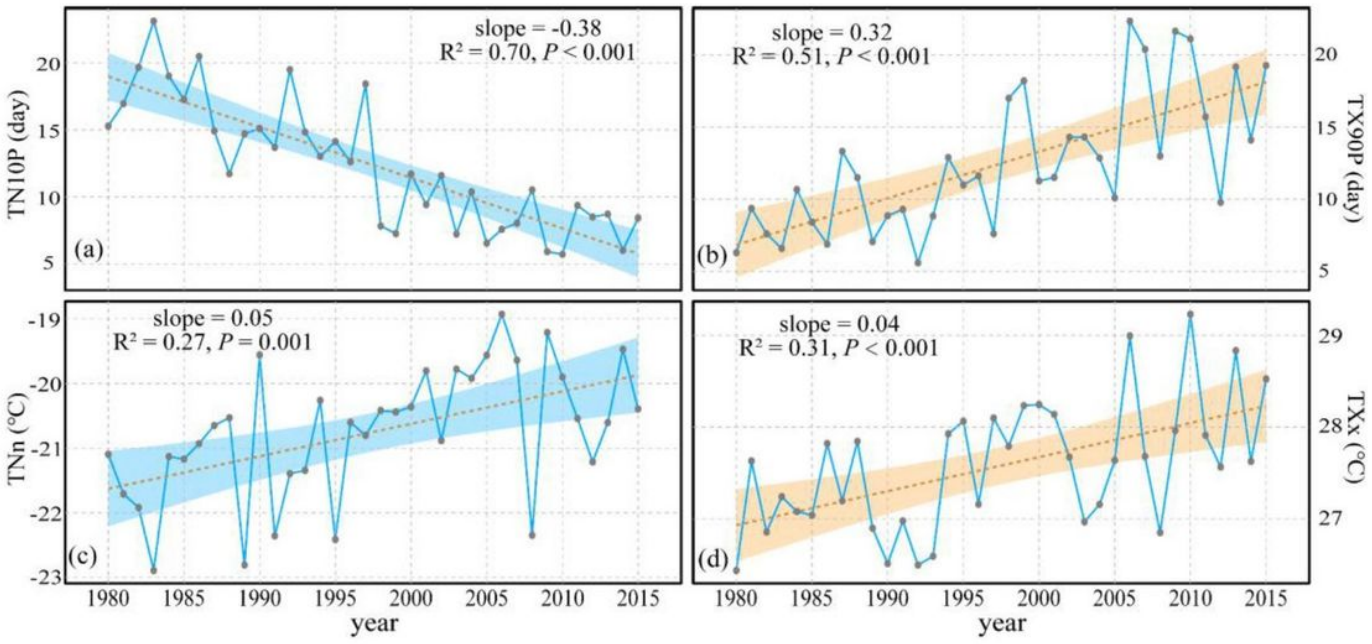

Figure 2

Linear regression trends for regional annual extreme temperature indices on TP during 1980-2015. (a) TN10p, (b) TX90p, (c) TNn, and (d) TXx. The blue line is the annual series of the considered index, and the dashed orange line is the linear trend.

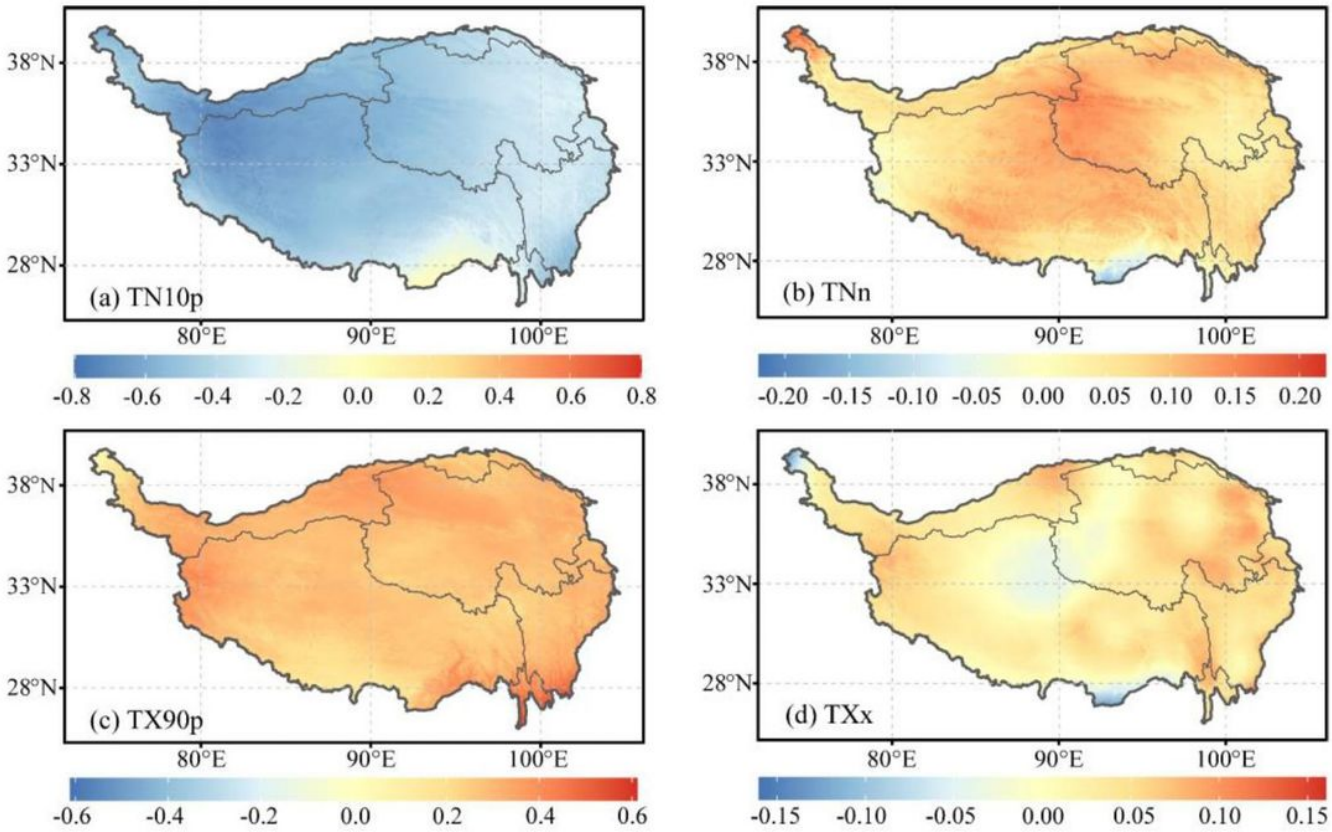

Figure 3

Spatial patterns of the annual trends in indices of extreme temperature events on the TP during 1980–2015. (a) TN10p (unit: day), (b) TNn (unit: ℃), (c) TX90p (unit: day), and (d) TXx (unit: ℃).

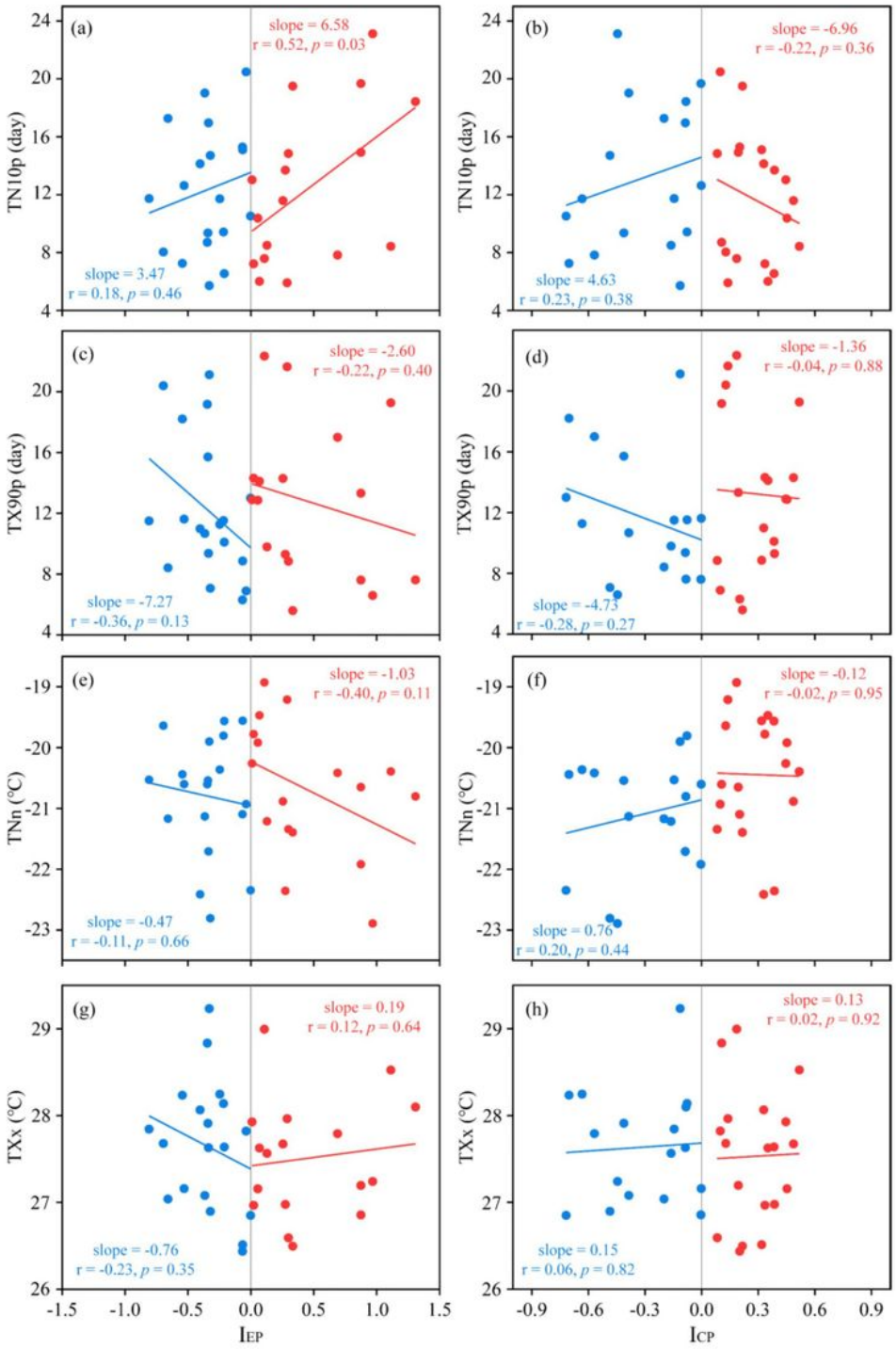

Figure 4

Response relationships between extreme temperature indices on y-axes and IEP (ICP) on x-axes for the period of 1980–2015. TN10p with (a) IEP and (b) ICP; TX90p with (c) IEP and (d) ICP; TNn with (e) IEP and (f) ICP; TXx with (g) IEP and (h) ICP. The blue and red dots are for the years with IEP (ICP) < 0 and IEP (ICP) > 0, respectively. The best fit lines, calculated using ordinary least squares regression, are shown with corresponding slope values. Pearson's correlation coefficient (r) and the significance of the fit (p) were calculated using the t-test.

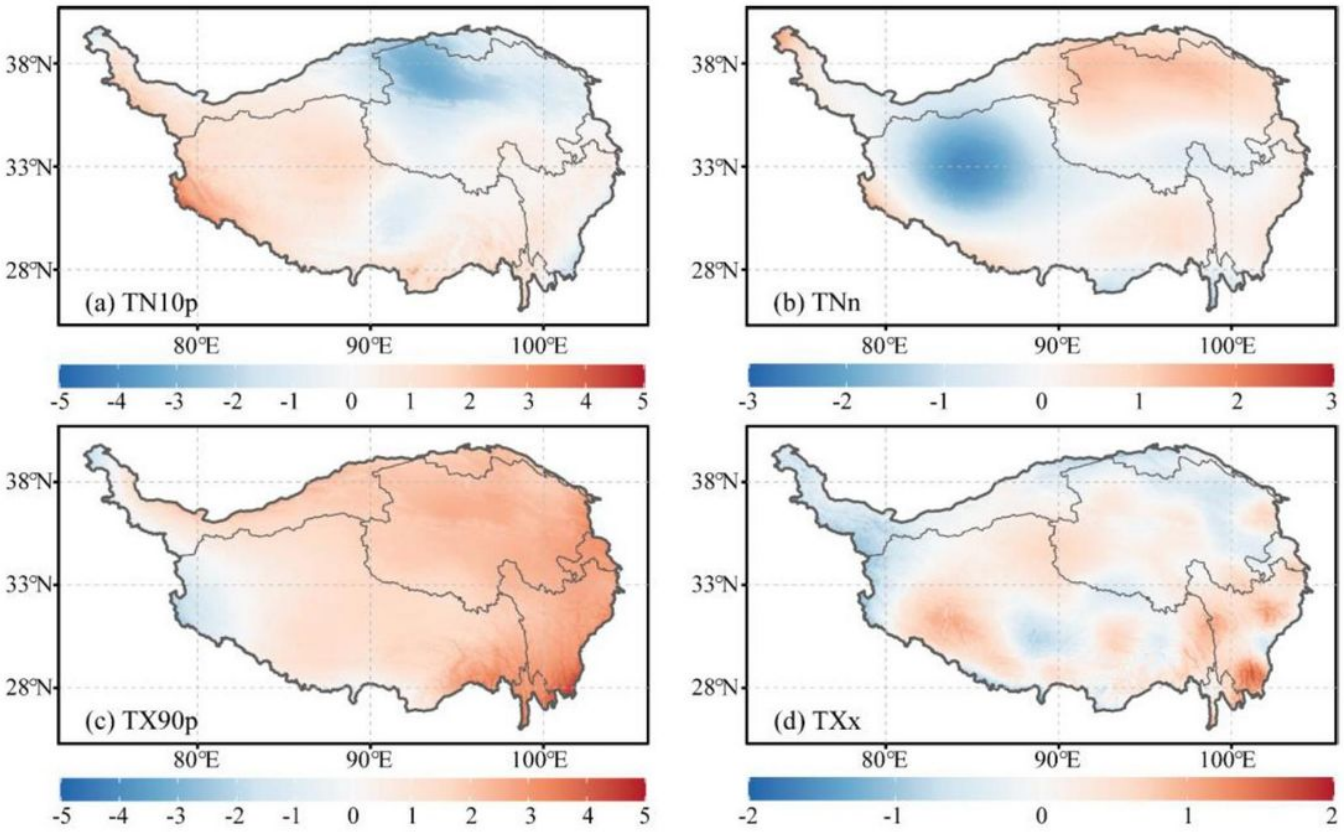

Figure 5

Composite analysis of extreme temperature indices in the EP E1 Niño years (Thigh - Tmean). (a) the differences in TN10p (unit: day), (b) the differences in TNn (unit: ℃), (c) the differences in TX90p (unit: day), and (d) the differences in TXx (unit: ℃).

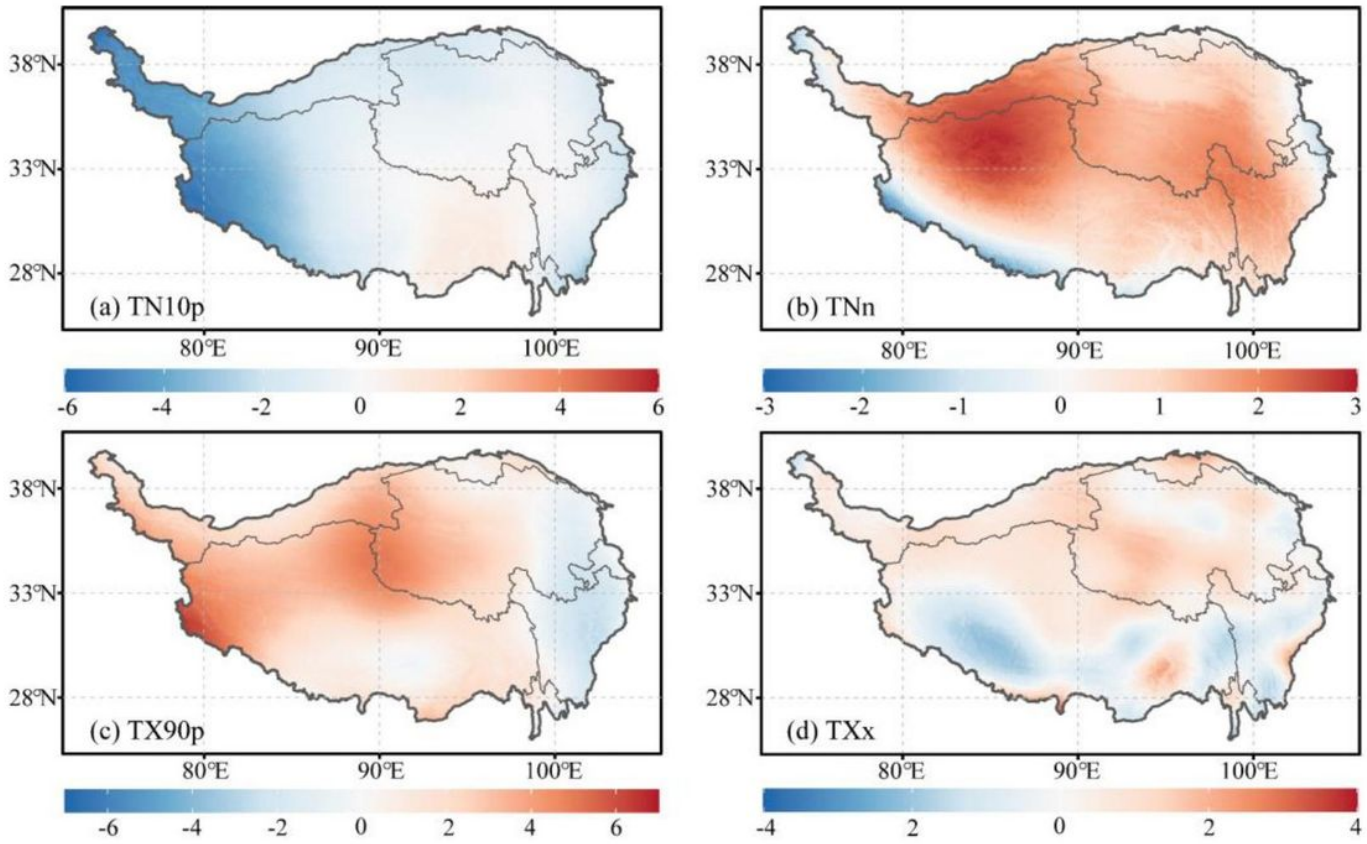

Figure 6

Composite analysis of extreme temperature indices in the CP E1 Niño years (Thigh - Tmean). (a) the differences in TN10p (unit: day), (b) the differences in TNn (unit: ℃), (c) the differences in TX90p (unit: day), and (d) the differences in TXx (unit: ℃).

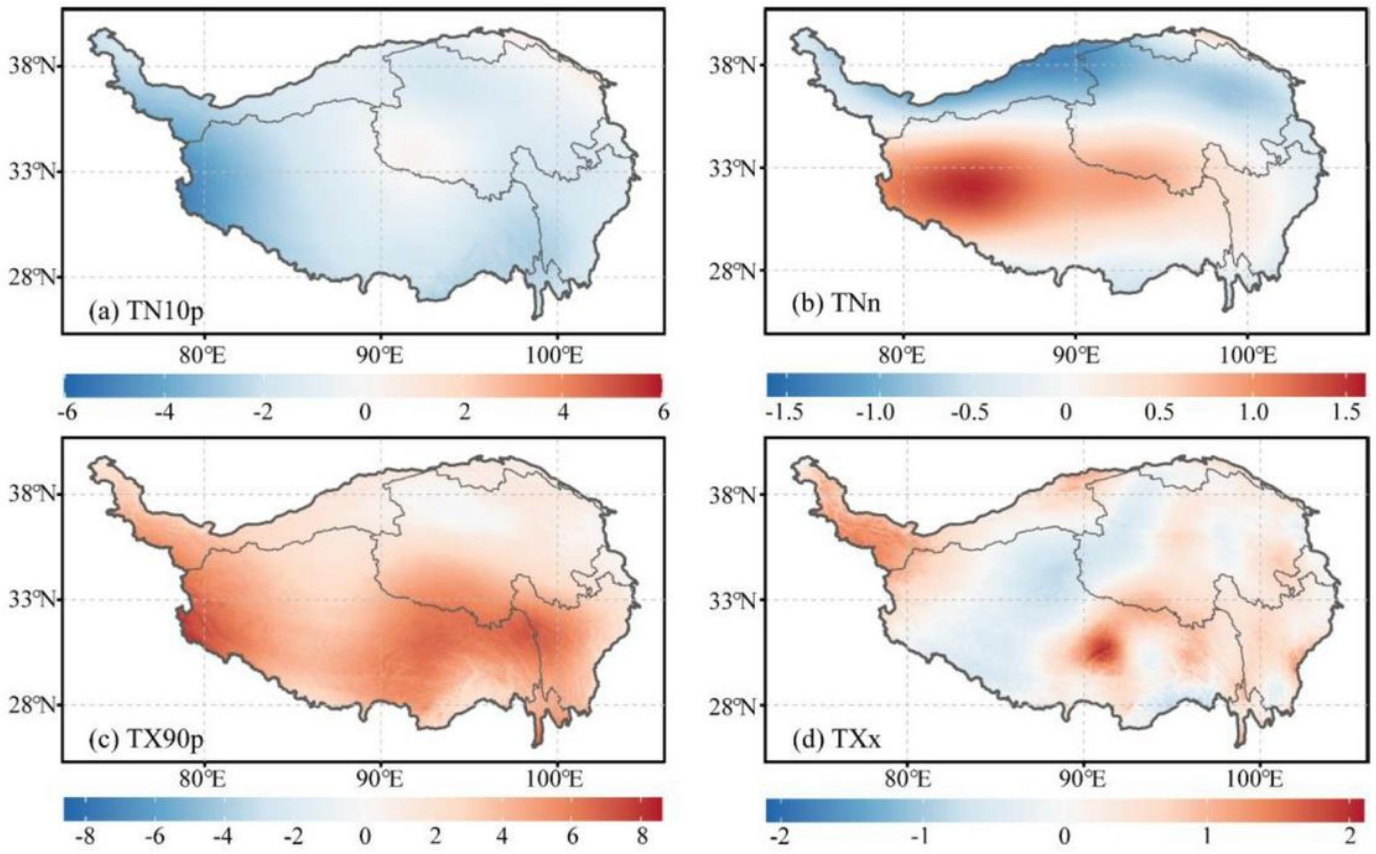

Figure 7

Composite analysis of extreme temperature indices in the EP La Niña years (Tlow - Tmean). (a) the differences in TN10p (unit: day), (b) the differences in TNn (unit: ℃), (c) the differences in TX90p (unit: day), and (d) the differences in TXx (unit: ℃).

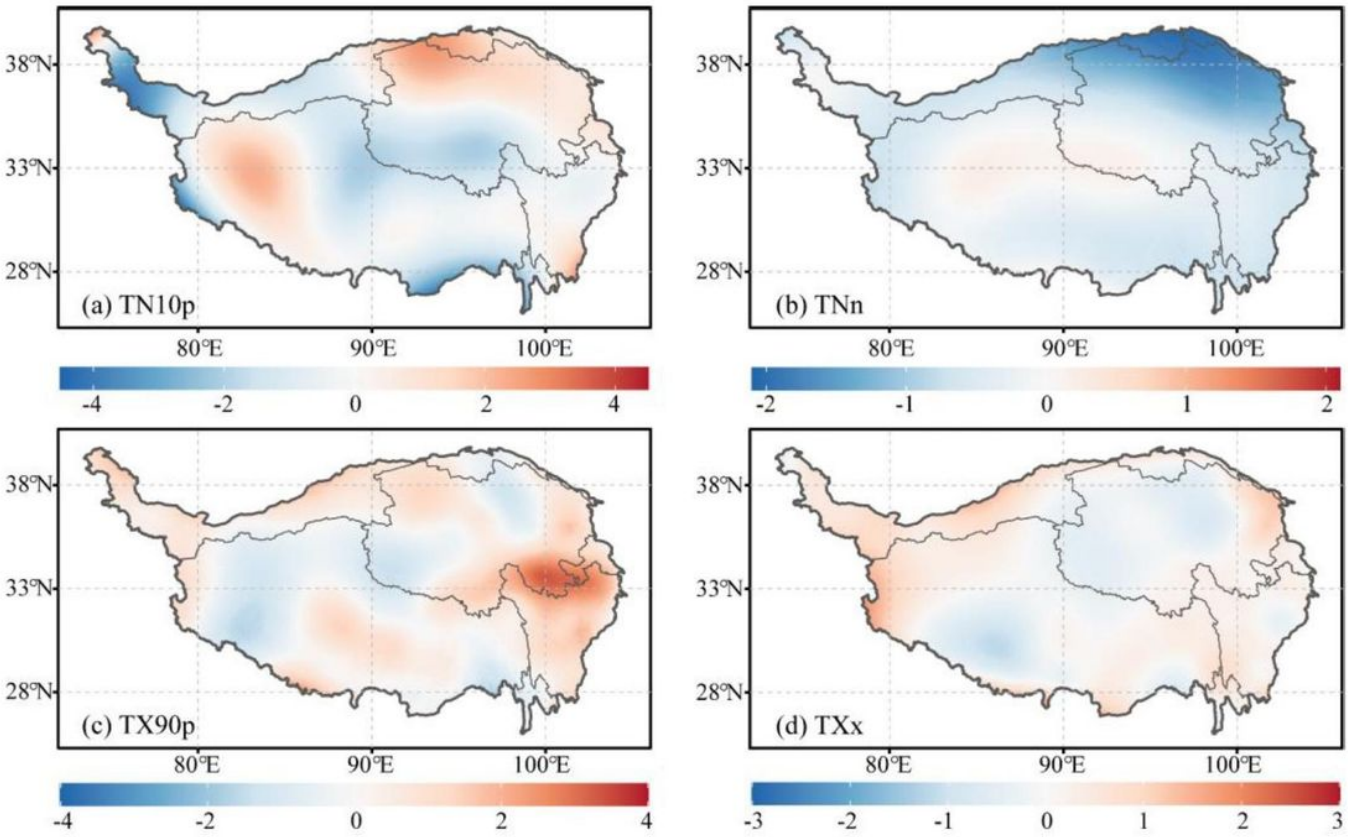

Figure 8

Composite analysis of extreme temperature indices in the CP La Niña years (Tlow - Tmean). (a) the differences in TN10p (unit: day), (b) the differences in TNn (unit: ℃), (c) the differences in TX90p (unit: day), and (d) the differences in TXx (unit: ℃).

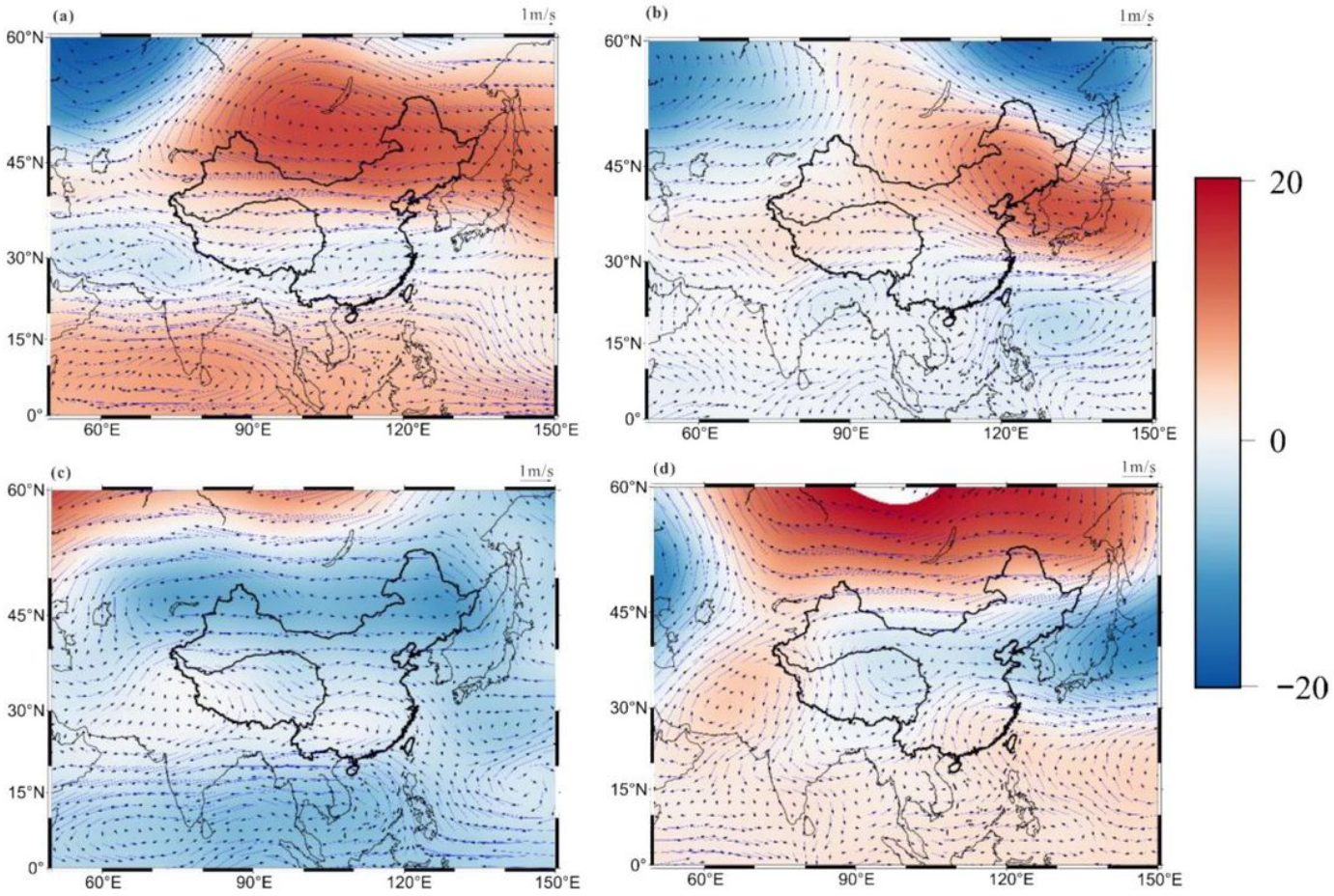

Figure 9

Changes in the average wind speed (arrows) and geopotential height (shading, unit: gpdam) at 500 hPa during the different types of ENSO events. (a) The average wind speed and geopotential height during the EP El Niño years minus those during the base period (1980–2010); (b) The average wind speed and geopotential height during the CP El Niño years minus those during the base period (1980–2010); (c) The average wind speed and geopotential height during the EP La Niña years minus those during the base period (1980–2010); (d) The average wind speed and geopotential height during the CP La Niña years minus those during the base period (1980–2010). The lengths of the arrows indicate the changes in the wind speed.

Supplementary Files

This is a list of supplementary files associated with this preprint. Click to download.

- Supplementmaterials.docx